



Synthesis, Structural and Fractal analysis of BFO Nanoparticles

Vivek Kumar Bajpai¹, Ajeet Kumar Rai¹ R.R. Awasthi^{2*}

¹Department VIAET, Mechanical Engineering, Shuats, Prayagraj-211007

²Faculty of Engineering and Technology, KhwajaMoinuddin Chishti Language University
Lucknow, 226013, (U.P.) India
Email:bajpai.vivek4@gmail.com

Article History

Volume 6, Issue 12, 2024

Received: 30 May 2024

Accepted : 30 June 2024

Doi:

10.48047/AFJBS.6.12.2024.2026-2033

Abstract

The main objective of the present investigation to examine the impact of annealing temperature varying from 450 °C to 500 °C on bismuth ferrite (BFO) thin films prepared by spray pyrolysis method. The X-ray diffraction (XRD) confirmed that BFO has typical rhombohedral phase with no intermediate impurity phases present in the sample. The average crystallite sizes as calculated using Scherer's equation found to be in the range of ~15 to 20 nm. The crystallite size and microstrain as calculated from Williamson-Hall methods were found to be ~17.67 nm, 22.35 nm, 28.54 nm and 0.028, 0.021 respectively. The atomic force microscopy (AFM) revealed that BFONPs are formed nanorods shape topography, symmetrically distributed throughout on the surface of the films. The surface roughness increases from ~4.56 nm to 7.68 nm with increase in the annealing temperature, indicating modified crystal structure of thin films. The fractal dimension values were observed and found to be 1.64 and 1.96. It can be seen that, increasing values of the fractal dimension with increasing annealing temperature 450 °C to 500 °C respectively. This result indicates that it can be employed to describe the variation of the entire grain morphology along the direction of growth. Also, unlike RMS roughness, the fractal dimension contains spatial information and profile deviation information.

Keywords: Multiferroics; fractal dimension; BFO; XRD; AFM

1. Introduction

During the last few decades, multiferroic materials have attracted considerable attention, due to their coupling ferroelectric and antiferromagnetic orders in the same phase [1,2]. Consequently, the discovery of the magnetoelectric (ME) effect has been considered to be promising for potential applications towards developing new kind of functional devices. There are very few energy-efficient single phase multiferroic materials that exist at room temperature [3]. The preparation of single phase nano-structured powders is essential to enhance the ferroelectric and magnetic properties. Multiferroic bismuth ferrite (BiFeO₃), which is commonly called as BFO is a popular bismuth-based material, which holds an excellent ferroelectric order and is widely used in high temperature magnetoelectric coupling devices. Currently, various advanced techniques have been reported to prepare multiferroic materials, which can tailor the surface area

to volume ratio and improve the microstructural and magnetic properties. The popular examples of such techniques are solid state reaction, sol-gel, hydrothermal [4-9] method etc.

BFO's intrinsic issues, such as high leakage, high loss, low polarization, variable oxidation state (+2, +3, +4) of Fe, and associated phases (Bi-rich phases: Bi_2O_3 and $\text{Bi}_{25}\text{FeO}_{39}$, Fe-rich phases: $\text{Bi}_2\text{Fe}_4\text{O}_9$ and Fe_2O_3) etc. hinder its commercial utilization. It is also predicted that substitution of Fe ions with 3d transition ions like Cr, Mn, Co, Ni and Cu increases the magnetic moments as well as magnetic anisotropies and hence improve the magnetic, optical and ferroelectric properties of BFO nanostructure [10-14]. Some transition elements (Mn, Zn, Ti, Al, etc.) are used to substitute Fe to reduce the large leakage current and improve the surface topography [15]. On the other hand some metal oxides nanostructures have been extensively used in present scenario but its limited application in functional device [16-18]. In the present research paper we have examined the impact of annealing temperature on bismuth ferrite (BFO) thin films prepared by spray pyrolysis method.

2. Experimental

High purity chemicals used were bismuth nitrate $\text{Bi}(\text{NO}_3)_3 \cdot 5\text{H}_2\text{O}$ ($\geq 99\%$, Merck) and iron nitrate $\text{Fe}(\text{NO}_3)_3 \cdot 9\text{H}_2\text{O}$ ($\geq 99\%$, Merck). These materials were weighed accurately in suitable stoichiometric amounts. Iron nitrate and bismuth nitrate were dissolved in 1:1 molar ratio. The precursor solution was continuously stirred for 2 hours at 70°C to obtain uniform, transparent precursor solution. The glass substrates were also cleaned with organic solvents methanol and acetone to remove dust particle/contaminant present on the glass surface. Finally, the precursor solutions were sprayed with the help of a nebulizer on the glass substrates at 400°C for 5 minutes, maintaining solution flow rate of 0.2 ml/min. The as synthesized thin films were annealed using a SiC furnace in an open-air environment for 3 hours at 450°C to 500°C in order to obtain appropriate crystallization. The structural and morphological properties of pure BFO nanomaterials were characterized by X-ray diffraction (XRD) using Rigaku ultima IV ($\text{CuK}\alpha$ $\lambda \sim 1.5404 \text{ \AA}$) and atomic force microscopy (AFM) Nanomagnetic Instrument.

3. Results and discussion

3.1. Structural analysis

Figure 1(a) depicts the XRD pattern of BFO nanostructures. The observed XRD peaks match well with the JCPDS (072-2112) of rhombohedral phase with R-3m space group. There are no intermediate impurity phases visible in the XRD pattern of BFO. The average crystallite sizes of BFO thin films annealed at 450°C to 500°C were determined using Scherer's equation; $D = \frac{K\lambda}{\beta \cos \theta}$, where K is constant ($K = 0.9$), λ is the X-ray wavelength of $\text{CuK}\alpha$ used in XRD, θ is the Bragg's angle and β is the full-width at half-maximum (FWHM). The average crystallite size was calculated using Scherer's equation found to be in the range of $\sim 15.4 \text{ nm}$ to 20.7 nm .

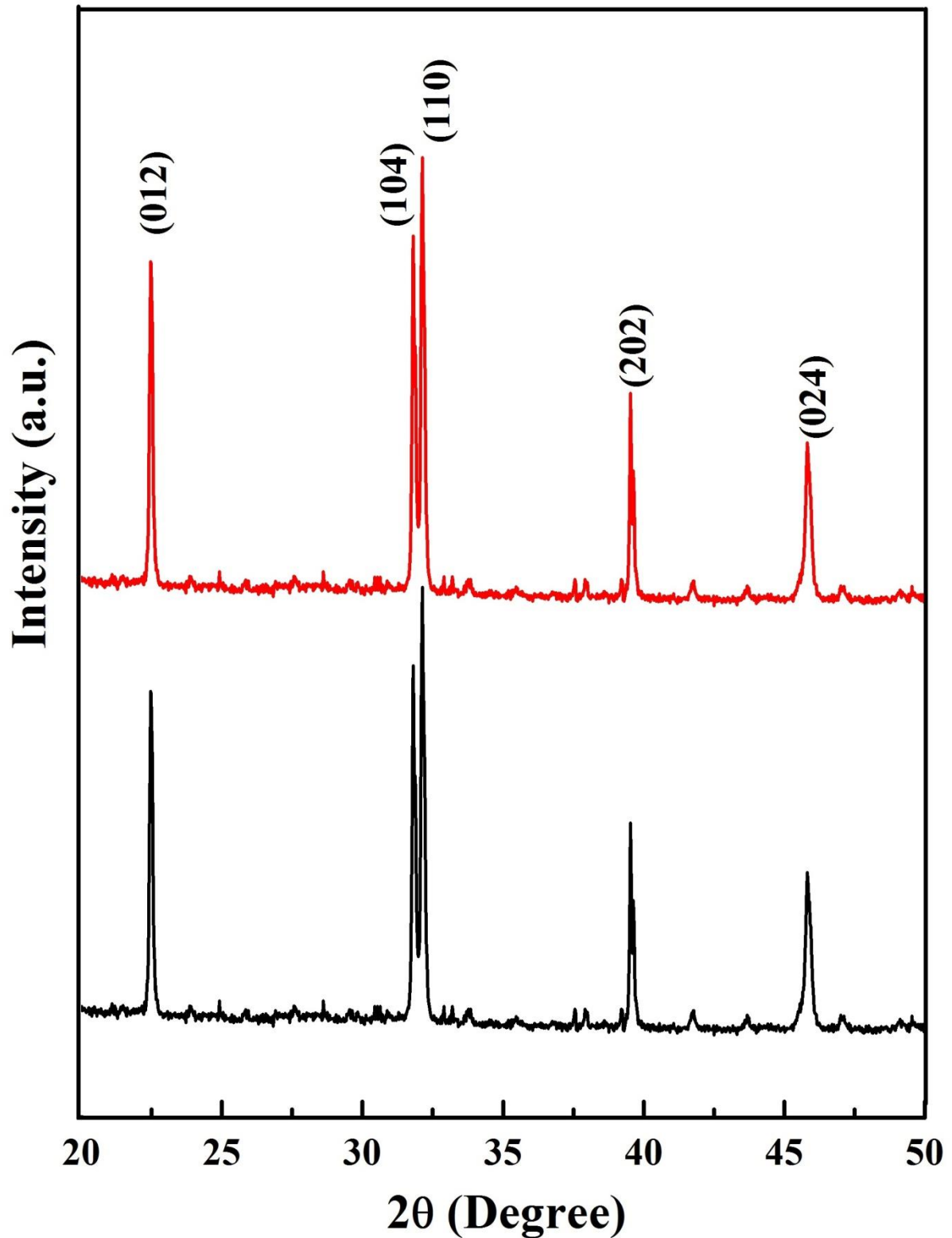


Figure 1 X-ray diffraction patterns of BFO thin films annealed at 450 °C and 500 °C. The micro strain and crystallite size are also calculated from Williamson-Hall (W-H) plot with

following relation $\beta \cos \theta = \frac{k\lambda}{D} + 4\epsilon \sin \theta$ Figure 2 shows W-H plot of graph plotted against

$\beta \cos \theta$ versus $4 \sin \theta$, gives the value of lattice strain (ϵ) and inverse of intercept gives the

value of crystallite size (D) corresponding to zero stain. The crystallite size and microstrain as calculated from Williamson-Hall methods were found to be ~ 17.67 nm, 22.35 nm 28.54 nm and 0.028 , 0.021 respectively.

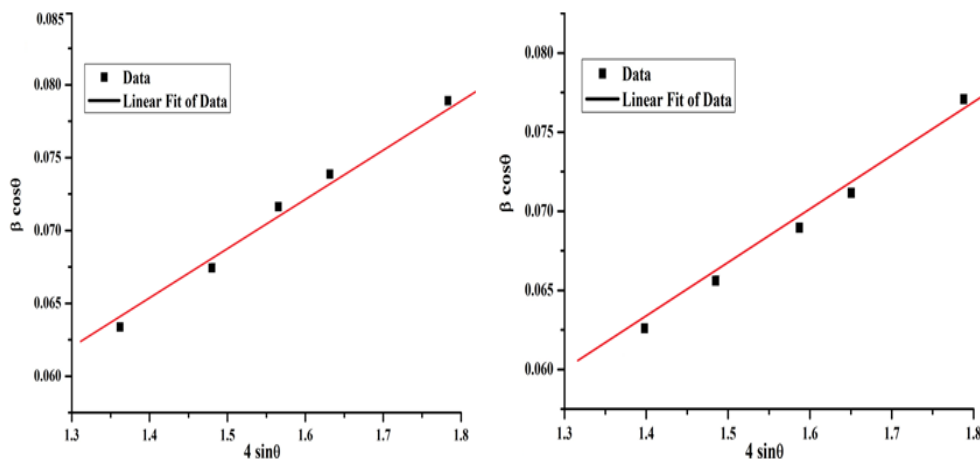


Figure 2(a-b) Williamson-Hall plot of BFO thin films annealed at 450 °C and 500 °C.

3.2. Surface topography

3.2.1 Atomic force microscopy (AFM) studies

Figure 2(a)-(b) exhibits the AFM images of BFO thin films prepared by spray pyrolysis technique carried out by atomic force microscopy (AFM) technique. The micrograph reveals that the formation of nanorods shape topography with granular growth of BFO thin films. The nanorods shape topography of BFO thin films distributed throughout the sample surface with clear grain and grain boundaries. Furthermore increase the annealing temperature the density and growth of nanorods shape topography of the film increases as shown in figure 2(a-b). The particle sizes as estimated from AFM image of BFO sample annealed at 450 °C and 500 °C were found to be about ~ 150 nm and ~ 200 nm respectively. Thus, increases the particles size with increasing of annealing temperature are well consistent with the obtained from the X-RD measurements. The surface parameters, such as root mean square (RMS) surface roughness of BFO thin films annealed at 450 °C and 500 °C were calculated and found to be ~ 4.56 nm to 7.68 nm respectively. This increase in roughness with increasing annealing temperature is indicating the enhancement of surfaces defect in of the BFO thin films.

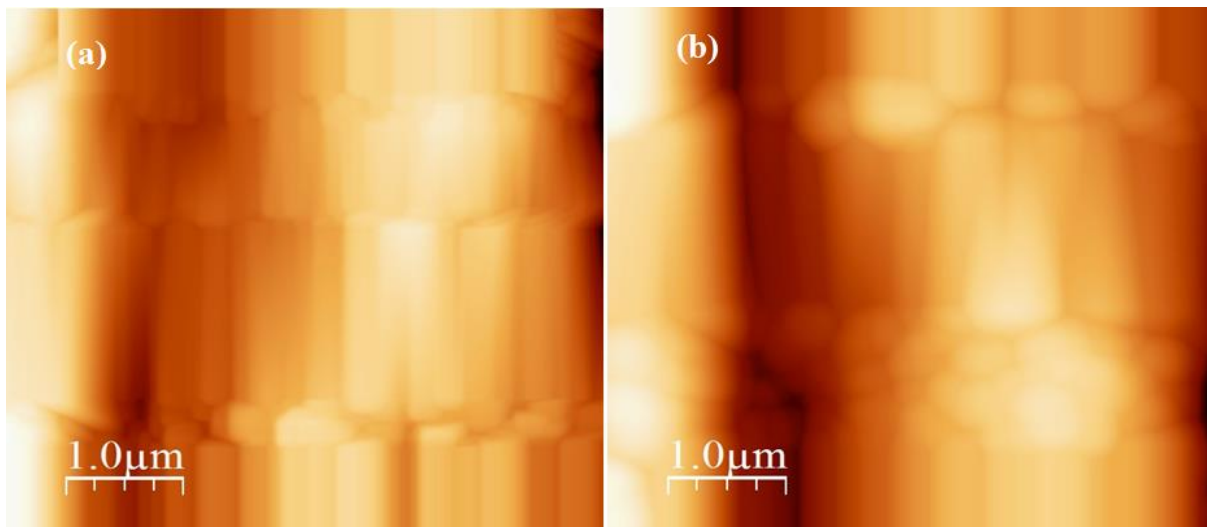


Figure 2(a-b) 2-D AFM surface topography of BFO thin films annealed at 450 °C and 500 °C. Figure 2(c)-(d) exhibited the high resolution contour plot of AFM images, which demonstrate that BFO thin films have symmetric growth of grains in-plane shapes with elliptical bases. Furthermore increases the annealing at 450 °C to 500 °C BFO thin film contour plot clearly revealed that enhance the symmetric growth and increase the in-plane shapes with elliptical bases.

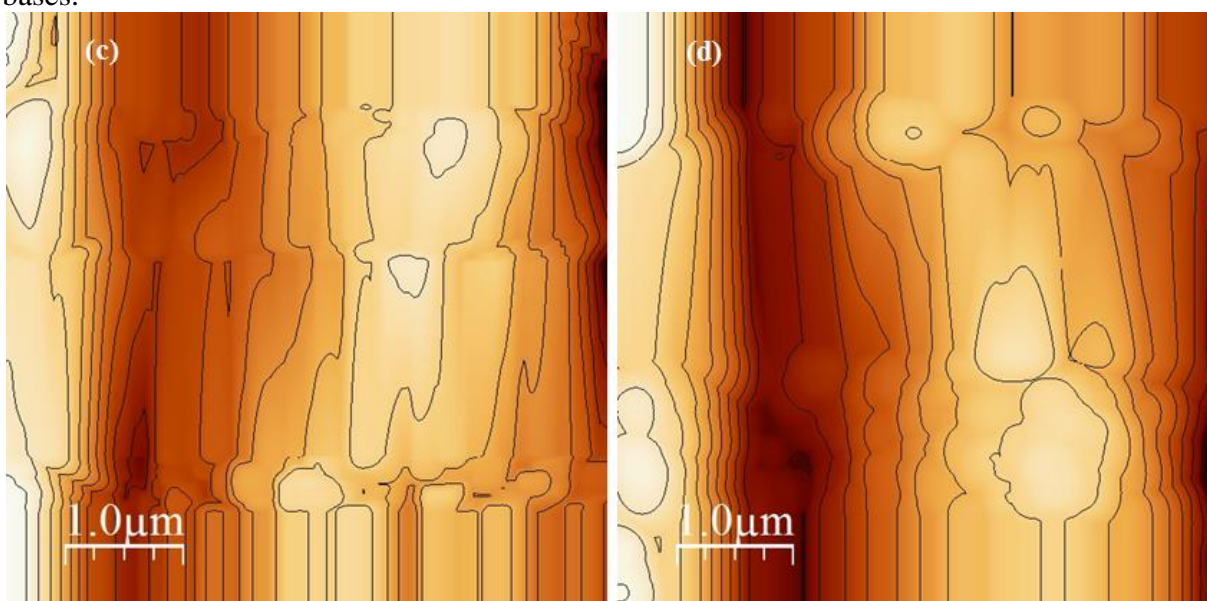


Figure 2(c-d) Contour plot of BFO thin films annealed at 450 °C and 500 °C.

Fig. 2(e) & 2(f) exhibit the 3-D AFM images, which demonstrate that BFO NPs have uniform grains of nanorods distribution with average height of 716.7 nm and 726.1 nm. The modification and small increment of Z-height distribution may be caused due to creates of lattice strain. Hence, it can be used fractal analysis to analysis of the grain distribution quantitatively and gives information about the random distribution of the grain.

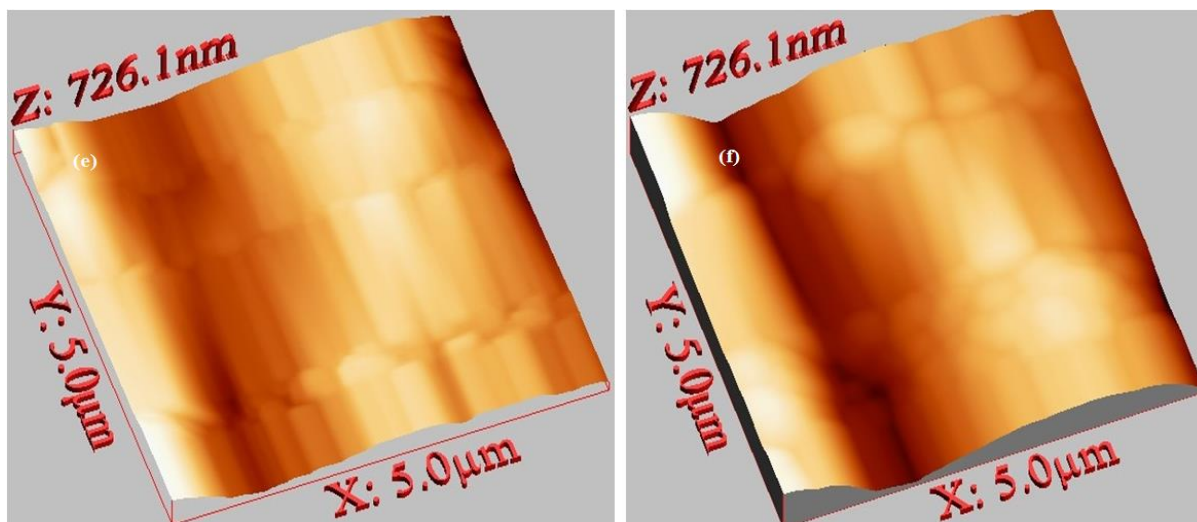


Figure 2(e-f) 3-D AFM image of BFO thin films annealed at 450 °C and 500 °C.

3.2.2 Fractal Analysis

Figure 3(a) & 3(b) exhibit fractal analyses of BFO materials using Power spectral density (PSD) method with increasing annealing temperature from 450 °C to 500 °C of BFO sample. The advantages of the fractal approach are the possibility of considering the complex fracture morphology of the surfaces. The fractal dimension is a possible measure of degree of surface roughness and depends on spatial distribution of grain within the thin film, crystal size and the combined effects of morphology. Power spectral density (PSD) method can be employed to calculate fractal dimension. In this method, fractal dimension (D) ranging from 2 to 3 is useful to reveal the irregularity of the surface morphology, and a larger D indicates a more irregular and fragmenting surface [19]. PSD method is based on the assumption that a fractal surface morphology is superimposed by the infinite frequency mode. The relationship of power spectrum density S_ω and the corresponding frequency ω depends on D . The values of S_ω and ω have relationship as follows:

$$S_\omega \propto \omega^{-(5-2D)}$$

Where D is fractal dimension of the film, the experimental surface is fractal at defined lengthscales of fractal behavior. Outside of these lengths the surface behaves like a flat surface.

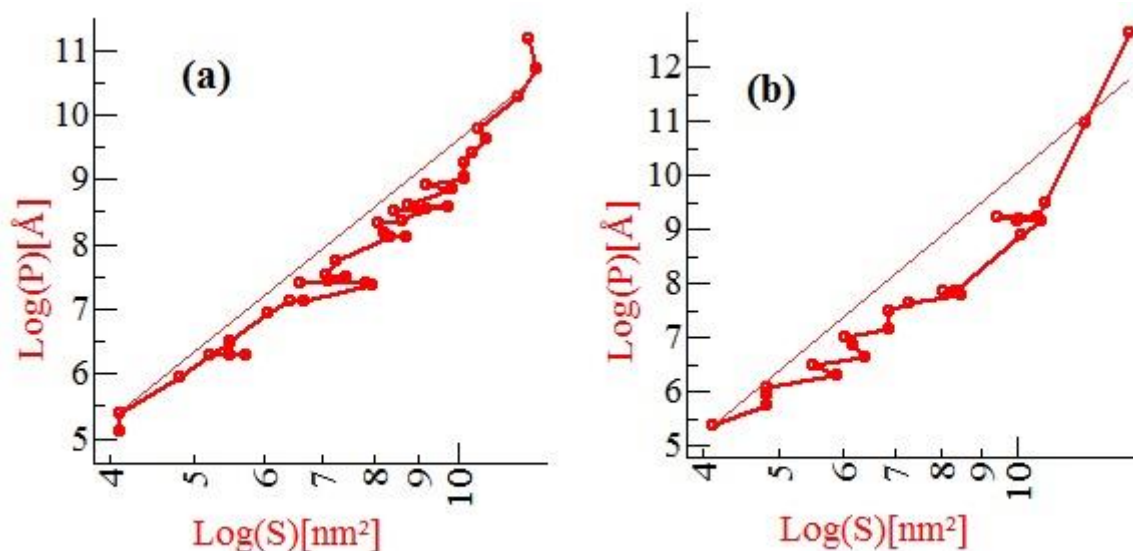


Figure 3 Fractal analyses of BFO thin films annealed at 450 °C and 500 °C using Power spectral density (PSD) method.

It can clearly observed fractal dimension values 1.64 and 1.96 be seen that, increasing values plough the fractal dimension. This result indicates that can be employed to describe the variation of theentire grain morphology along direction of the growth. Also, unlikeRMS roughness, the fractal dimension contains spatial information andprofile deviation information. So, the fractal analysis provides a usefuldescription of the irregularities in the surface. As mentioned above,fractal analysis is more accurate than conventional processing due tocalculate the fractal dimension in every scaling range.

4. Conclusion

In present work, we have successfully fabricated BFO thin films prepared by spray pyrolysis method. The XRD confirm single phase formation of BFO thin films with rhombohedral crystal structurewith R-3m space group. The average crystallite sizes as calculated using Scherer's equation found to be in the range of ~15 to 20 nm. The crystallite size and microstrain as calculated from Williamson-Hall methods were found to be ~17.67 nm, 22.35 nm 28.54 nm and 0.028, 0.021 respectively.The RMS surface roughness increases from ~4.56 nm to 7.68 nm with increase the annealing temperature indicates modified the crystal structure of thin films. The fractal dimension values observed from AFM image and found to be 1.64 and 1.96 be seen that, increasing the fractal dimensionwith increasing annealing temperature from 450 °C to 500 °C of sample. This result can be employed to describe the variation of theentire grain morphology along direction of the growth. Also, unlikeRMS roughness, the fractal dimension contains spatial information andprofile deviation information.The decrement in RMS surface roughness by increasing annealing temperature with increasing annealing temperature from 450 °C to 500 °C of BFO sampleindicates that the material can have potential applications multiferroic materials baseddevices.

Acknowledgements

The authors are highly thankful to Department of Physics, University of Lucknow, Lucknow for providing X-RD and AFM measurement.

References

- [1] G. Lawes and G. Srinivasan, Introduction to magnetoelectric coupling and multiferroic films, J. Phys. D Appl. Phys. 44 (2011) 243001–243022.

- [2] J. Ma, J. Hu, Z. Li, and C.W. Nan, Recent progress in multiferroic magnetoelectric composites: From bulk to thin films, *Adv. Mater.* 23(9) (2011) 1062–1087.
- [3] C.C. Zhou, B.C. Luo, K.X. Jin, X.S. Cao, and C.L. Chen, Magnetic and dielectric properties of $\text{BiFeO}_3\text{-La}_{1/3}\text{Sr}_{2/3}\text{MnO}_3$ hybrid composite ceramics, *Solid State Commun.* 150 (2010) 1334-1337.
- [4] A.K. Singh, S.D. Kaushik, B. Kumar, P.K. Mishra, A. Venimadhav, V. Siruguri, and S. Patnaik, Substantial magnetoelectric coupling near room temperature in $\text{Bi}_2\text{Fe}_4\text{O}_9$, *App.Phys. Lett.* 92 (2008) 132910-132913.
- [5] H. Koizumi, N. Niizeki, and T. Ikeda, An X-ray study on $\text{Bi}_2\text{O}_3\text{-Fe}_2\text{O}_3$ system, *Jpn. J. Appl. Phys.* 3 (1964) 495-496.
- [6] T. Liu, Y. Xu, and C. Zeng, Synthesis of $\text{Bi}_2\text{Fe}_4\text{O}_9$ via PVA sol-gel route, *Mater. Sci. Eng. B* 176 (2011) 535-539.
- [7] Z. Yang, Y. Huang, B. Dong, H.L. Li, and S.Q. Shi, Densely packed single-crystal $\text{Bi}_2\text{Fe}_4\text{O}_9$ nanowires fabricated from a template-induced sol-gel route, *J. Solid State Chem.* 179 (2006) 3324-3329.
- [8] Y. Xiong, M.Z. Wu, Z. M. Peng, N. Jiang and Q.W. Chen, Hydrothermal synthesis and characterization of $\text{Bi}_2\text{Fe}_4\text{O}_9$ nanoparticles, *Chem. Lett.* 33 (2004) 502–503.
- [9] Y. G. Wang, G. Xu, L. L. Yang, Z. H. Ren, X. Wei, W. J. Weng, P. Y. Du, G. Shen and G. R. Han, Low temperature polymer assisted hydrothermal synthesis of bismuth ferrite nanoparticles, *Ceram. Int.* 35 (2009) 51–53.
- [10] R.R. Awasthi, B. Das, Structural transition and tunable optical, morphological and magnetic properties of Mn-doped BiFeO_3 films, *Optik* 194 (2019) 162973.
- [11] R.R. Awasthi, K. Asokan, B. Das, Structural, dielectric and magnetic domains properties of Mn-doped BiFeO_3 materials, *International Journal of Applied Ceramic Technology* 17 (2020) 1410.
- [12] H. Naganuma, J. Miura, and S. Okamura, Ferroelectric, Electrical and Magnetic Properties of Cr, Mn, Co, Ni, Cu Added Polycrystalline BiFeO_3 films, *Appl. Phys. Lett.* 93 (2008) 052901.
- [13] R.R. Awasthi, K. Asokan, B. Das, Effect of molar concentration on structural, magnetic domain and optical properties of BiFeO_3 thin films *Applied Physics A* 125 (2019) 338.
- [14] R.R. Awasthi, B. Das, Effect of temperature on physical properties of $\text{Bi}_2\text{Fe}_4\text{O}_9$ polycrystalline materials, *Journal of the Australian Ceramic Society* 56 (1) (2020) 243.
- [15] R.R. Awasthi, S.K. Trivedi, V.S. Chandel, M. Shariq, H.J. Alathlawi, S.P. Singh, Effect of Zn doping on structural/microstructural, surface topography, and dielectric properties of $\text{Bi}_2\text{Fe}_4\text{O}_9$ polycrystalline nanomaterials. *ACS omega.* 8(2023)15960-15967.
- [16] K.C. Dubey, A Zaidi, R.R Awasthi, Environmentally benign structural, topographic, and sensing properties of pure and Al-doped ZnO thin films. *ACS omega.* 7 (2022)28946-28954.
- [17] A Zaidi, K. Tiwari, R.R Awasthi, K.C. Dubey, Effect of sintering temperature on the structural, morphological and humidity sensing properties of ZnO nanostructure. *Journal of Ovonic Research* 19 (2023) 411-419.
- [18] A Zaidi, K. Tiwari, R.R Awasthi, K.C. Dubey, Effect of pH values on the structural, morphological and sensing properties of ZnO nanostructure. *Chalcogenide Letters* 20 (2023) 33-41.
- [19] C.L. Jing, W. Tang, Ga-doped ZnO thin film surface characterization by wavelet and fractal analysis, *Appl. Surf. Sci.*, 364 (2016) 843-849.